Bioconjugate Chemistry

Article

pubs.acs.org/bc

Impact of Multiple Negative Charges on Blood Clearance and Biodistribution Characteristics of ^{99m}Tc-Labeled Dimeric Cyclic RGD Peptides

Yong Yang, Shundong Ji, and Shuang Liu*

School of Health Sciences, Purdue University, 550 Stadium Mall Drive, West Lafayette, Indiana 47907, United States

ABSTRACT: This study sought to evaluate the impact of multiple negative charges on blood clearance kinetics and biodistribution properties of ^{99m}Tc-labeled RGD peptide dimers. Bioconjugates HYNIC-P6G-RGD$_2$ and HYNIC-P6D-RGD$_2$ were prepared by reacting P6G-RGD$_2$ and P6D-RGD$_2$, respectively, with excess HYNIC-OSu in the presence of diisopropylethylamine. Their IC_{50} values were determined to be 31 ± 5 and 41 ± 6 nM, respectively, against ^{125}I-echistatin bound to U87MG glioma cells in a whole-cell displacement assay. Complexes [^{99m}Tc(HYNIC-P6G-RGD$_2$)(tricine)(TPPTS)] (^{99m}Tc-P6G-RGD$_2$) and [^{99m}Tc(HYNIC-P6D-RGD$_2$)(tricine)(TPPTS)] (^{99m}Tc-P6D-RGD$_2$) were prepared in high radiochemical purity (RCP > 95%) and specific activity (37−110 GBq/μmol). They were evaluated in athymic nude mice bearing U87MG glioma xenografts for their biodistribution. The most significant difference between ^{99m}Tc-P6D-RGD$_2$ and ^{99m}Tc-P6G-RGD$_2$ was their blood radioactivity levels and tumor uptake. The initial blood radioactivity level for ^{99m}Tc-P6D-RGD$_2$ (4.71 ± 1.00%ID/g) was ∼5× higher than that of ^{99m}Tc-P6G-RGD$_2$ (0.88 ± 0.05%ID/g), but this difference disappeared at 60 min p.i. ^{99m}Tc-P6D-RGD$_2$ had much lower tumor uptake (2.20−3.11%ID/g) than ^{99m}Tc-P6G-RGD$_2$ (7.82−9.27%ID/g) over a 2 h period. Since HYNIC-P6D-RGD$_2$ and HYNIC-P6G-RGD$_2$ shared a similar integrin $\alpha_v\beta_3$ binding affinity (41 ± 6 nM versus 31 ± 5 nM), the difference in their blood activity and tumor uptake is most likely related to the nine negative charges and high protein binding of ^{99m}Tc-P6D-RGD$_2$. Despite its low uptake in U87MG tumors, the tumor uptake of ^{99m}Tc-P6D-RGD$_2$ was integrin $\alpha_v\beta_3$-specific. SPECT/CT studies were performed using ^{99m}Tc-P6G-RGD$_2$ in athymic nude mice bearing U87MG glioma and MDA-MB-231 breast cancer xenografts. The SPECT/CT data demonstrated the tumor-targeting capability of ^{99m}Tc-P6G-RGD$_2$, and its tumor uptake depends on the integrin $\alpha_v\beta_3$ expression levels on tumor cells and neovasculature. It was concluded that the multiple negative charges have a significant impact on the blood clearance kinetics and tumor uptake of ^{99m}Tc-labeled dimeric cyclic RGD peptides.

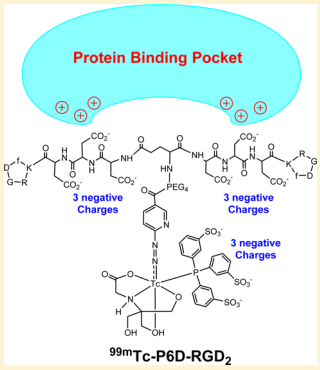

INTRODUCTION

Integrin $\alpha_v\beta_3$ plays a significant role in angiogenesis and tumor metastasis,[1−4] and is a receptor for extracellular matrix proteins (such as vitronectin, fibronectin, fibrinogen, laminin, collagen, Von Willebrand's factor, and osteoponin) with the arginine-glycine-aspartic (RGD) peptide sequence.[5] Over last several years, many radiolabeled (^{99m}Tc, ^{18}F, ^{64}Cu, ^{68}Ga, and ^{111}In) cyclic RGD peptides have been evaluated as radiotracers for tumor imaging by single photon emission computed tomography (SPECT) or positron emission tomography (PET),[6−25] and have been reviewed extensively.[26−30] The cyclic RGD peptides, such as E[c(RGDfK)]$_2$ (RGD$_2$), are targeting biomolecules to carry radionuclide to the integrin $\alpha_v\beta_3$ overexpressed on the tumor cells and/or tumor neovasculature. Multiple cyclic RGD peptides have been utilized to maximize their integrin $\alpha_v\beta_3$ binding affinity and the radiotracer tumor uptake. It was found that radiolabeled multimeric cyclic RGD peptides had significantly higher tumor uptake with longer tumor retention time than their monomeric counterparts.[28] The linkers between the two c(RGDfK) moieties in dimeric cyclic RGD peptides (Figure 1) are also important for their tumor-targeting capability and excretion kinetics of ^{99m}Tc radiotracers.

Many water-soluble linkers have been proposed to improve pharmacokinetics of radiolabeled cyclic RGD peptides.[28,31−33] For example, 7-amino-L-glycero-L-galacto-2,6-anhydro-7-deoxy-heptanamide (SAA) has successfully used to minimize the liver radioactivity accumulation and increase target-to-background ratios of ^{18}F-labeled cyclic RGD peptides.[6,10] The (cysteic acid)$_2$ dipeptide was utilized to minimize the liver uptake of radiolabeled integrin $\alpha_v\beta_3$ antagonists.[34−37] The hexaethylene glycol (HEG) has been incorporated in ^{18}F-labeled RGDfE dimers and tetramers.[7−9] It was reported that the polyethylene glycol (PEG) linkers could improve not only the tumor uptake but also the pharmacokinetics of radiolabeled c(RGDyK) and ^{64}Cu-labeled E[c(RGDyK)]$_2$.[11−13]

We have been using 15-amino-4,7,10,13-tetraoxapentadecanoic acid (PEG$_4$) and Gly-Gly-Gly (G$_3$) as linkers to maximize the tumor-targeting capability and improve excretion kinetics of ^{99m}Tc labeled cyclic RGD peptides.[38−48] In this study, we used the Asp-Asp-Asp (D$_3$) tripeptide sequence to prepare HYNIC-P6D-RGD$_2$ (HYNIC = 6-(2-(2-sulfonatobenzaldehyde)-

Received: July 14, 2014
Revised: August 7, 2014
Published: August 11, 2014

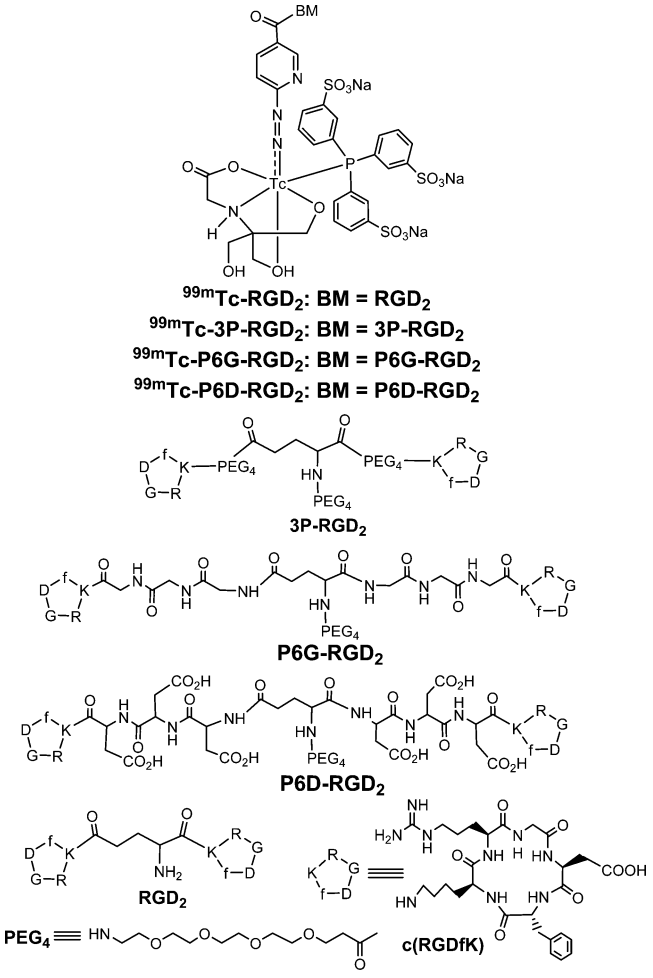

Figure 1. Chemdraw structures of cyclic RGD peptides (c(RGDfK), RGD_2, 3P-RGD_2, P6G-RGD_2, P6D-RGD_2, and their corresponding ternary ligand complexes [^{99m}Tc(HYNIC-BM)(tricine)(TPPTS)] (BM = biomolecule; ^{99m}Tc-RGD_2: BM = RGD_2; ^{99m}Tc-3P-RGD_2: BM = 3P-RGD_2; ^{99m}Tc-P6G-RGD_2: BM = P6G-RGD_2, ^{99m}Tc-P6D-RGD_2: BM = P6D-RGD_2).

hydrazono)nicotinyl; P6D-RGD_2 = PEG_4-E[c(RGDfK-(D_3))]$_2$). We were interested in P6D-RGD_2 because it contains two D_3 linkers with six carboxylic groups that could be deprotonated under physiological conditions (pH = 7.4). It was reported that the D_3 linker was able to minimize the liver radioactivity accumulation of ^{99m}Tc-labeled c(RGDfK).[49] For comparison purpose, we also prepared HYNIC-P6G-RGD_2 (P6G-RGD_2 = PEG_4-E[c(RGDfK(G_3))]$_2$) due to the neutral charges of G_3 tripeptide sequences. We evaluated the ternary ligand complexes [^{99m}Tc(HYNIC-P6G-RGD_2)(tricine)-(TPPTS)] (Figure 1: ^{99m}Tc-P6G-RGD_2) and [^{99m}Tc(HYNIC-P6D-RGD_2)(tricine)(TPPTS)] (^{99m}Tc-P6D-RGD_2) in the athymic nude mice bearing U87MG glioma xenografts to explore the impact of multiple negative overall molecular charges on blood clearance kinetics and biodistribution properties of ^{99m}Tc radiotracers. SPECT/CT studies were performed using ^{99m}Tc-P6G-RGD_2 in athymic nude mice bearing U87MG glioma and MDA-MB-231 breast cancer xenografts to demonstrate its utility as a radiotracer for tumor imaging.

RESULTS

Bioconjugate Synthesis. HYNIC-P6D-RGD_2 and HYNIC-P6G-RGD_2 were prepared by direct conjugation of P6D-RGD_2 and P6G-RGD_2, respectively, with HYNIC-OSu in the presence of excess DIEA. The reaction between P6D-RGD_2 and HYNIC-OSu was slow at room temperature (~15 days to complete). The reaction between P6G-RGD_2 and HYNIC-OSu was completed within 3 days at room temperature. It seems that the addition of six carboxylic groups between the two c(RGDfK) moieties make the conjugation reaction slower. HYNIC-P6D-RGD_2 and HYNIC-P6G-RGD_2 were purified by HPLC, and have been characterized by MALDI mass spectroscopy. The MS data were completely consistent with their proposed composition. Their HPLC purity was >95% before being used for the integrin $\alpha_v\beta_3$ binding assays and ^{99m}Tc-labeling.

Integrin $\alpha_v\beta_3$ Binding Affinity. Figure 2 shows the displacement curves of ^{125}I-echistatin bound to U87MG

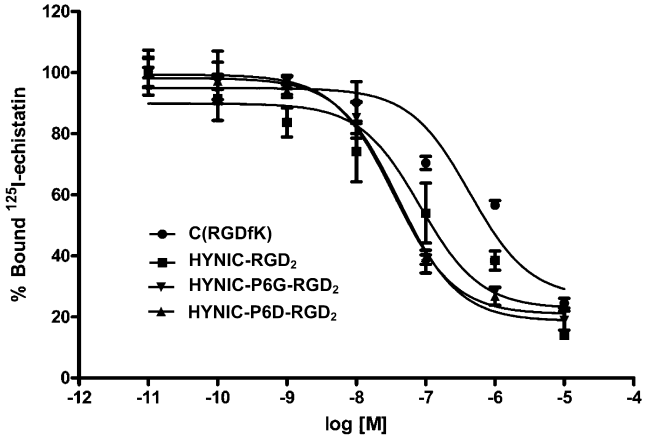

Figure 2. Competitive displacement curves of ^{125}I-echistatin bound to U87MG human glioma cells in the presence of cyclic RGD peptides. HYNIC-RGD_2 and c(RGDyK) were used for comparison purposes. IC_{50} values were calculated to be 32 ± 5, 41 ± 6, 85 ± 8, and 422 ± 15 nM for HYNIC-P6G-RGD_2, HYNIC-P6D-RGD_2, HYNIC-RGD_2, and c(RGDfK), respectively.

human glioma cells in the presence of cyclic RGD peptides. For comparison purposes, we also evaluated c(RGDyK) and HYNIC-RGD_2 in the same assay. IC_{50} values were calculated to be 31 ± 5, 41 ± 6, 85 ± 2, and 422 ± 15 nM for HYNIC-P6G-RGD_2, HYNIC-P6G-RGD_2, HYNIC-RGD_2, and c(RGDyK), respectively. The integrin $\alpha_v\beta_3$ binding affinity follows the order of HYNIC-P6G-RGD_2 ~ HYNIC-P6D-RGD_2 > HYNIC-RGD_2 ≫ c(RGDyK). The IC_{50} values of HYNIC-P6G-RGD_2 and HYNIC-P6D-RGD_2 were very close to that of HYNIC-3P-RGD_2 (IC_{50} = 32 ± 1 nM; 3P-RGD_2: PEG_4-E[PEG_4-c(RGKfD)]$_2$ and PEG_4 = 15-amino-4,7,10,13-tetraoxapentadecanoic acid) reported in our previous studies.[39,48] Apparently, replacing the two neutral G_3 or PEG_4 linkers with a pair of triple-charged D_3 tripeptide sequences did not significantly alter the integrin $\alpha_v\beta_3$ binding affinity of dimeric cyclic RGD peptides.

Radiochemistry. ^{99m}Tc-labeling was accomplished by heating the reaction mixture at 100 °C for 15−20 min. Figure 3 shows radio-HPLC chromatograms of ^{99m}Tc-P6D-RGD_2 and ^{99m}Tc-P6G-RGD_2 in the kit matrix. Their RCP was >95% without postlabeling chromatographic purification. The specific

dx.doi.org/10.1021/bc500309r | Bioconjugate Chem. 2014, 25, 1720−1729

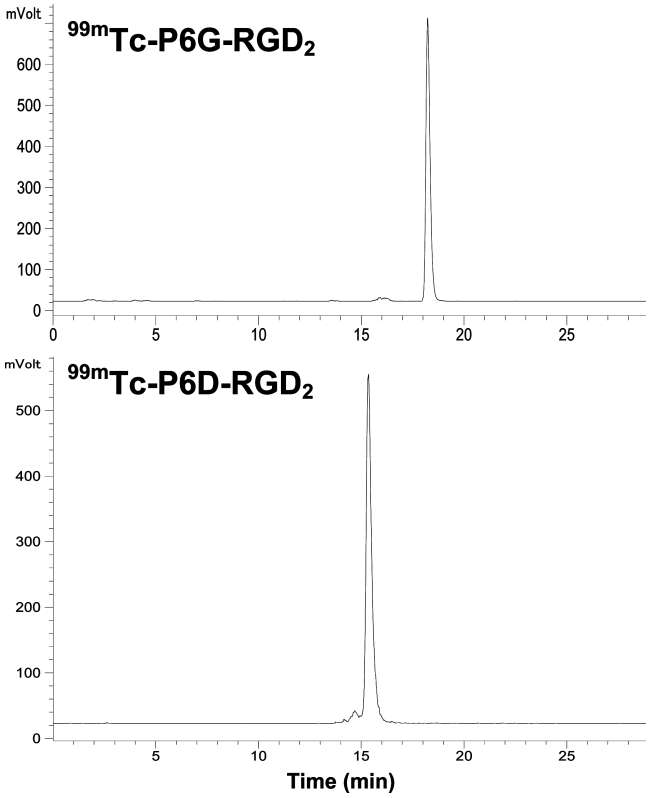

Figure 3. Typical radio-HPLC chromatograms of ^{99m}Tc-P6G-RGD$_2$ and ^{99m}Tc-P6D-RGD$_2$. Their RCP was >95% without postlabeling chromatographic purification.

activity was 37−110 GBq/μmol for ^{99m}Tc-P6D-RGD$_2$ and ^{99m}Tc-P6G-RGD$_2$. They both remained stable in the kit matrix for more than 6 h postlabeling.

Biodistribution Properties. Biodistribution studies were performed on ^{99m}Tc-P6D-RGD$_2$ and ^{99m}Tc-P6G-RGD$_2$ to compare their blood clearance, tumor uptake, and biodistribution properties in athymic nude mice bearing U87MG glioma xenografts. Tables 1 and 2 list the selected biodistribution data for ^{99m}Tc-P6D-RGD$_2$ and ^{99m}Tc-P6G-RGD$_2$, respectively. For comparison purposes, we also obtained the 5 and 60 min biodistribution data of ^{99m}Tc-3P-RGD$_2$ (Figure 1: [^{99m}Tc(HYNIC-3P-RGD$_2$)(tricine)(TPPTS)]), which is currently under clinical evaluations as a SPECT radiotracer for imaging integrin $\alpha_v\beta_3$-positive tumors.[50−52] It was found that the most significant difference between ^{99m}Tc-P6D-RGD$_2$ and ^{99m}Tc-P6G-RGD$_2$ was their blood activity levels and tumor uptake. The blood activity level of ^{99m}Tc-P6D-RGD$_2$ was 4.71 ± 1.00%ID/g, ∼5× higher than that of ^{99m}Tc-P6G-RGD$_2$ (0.88 ± 0.05%ID/g) and ∼3× higher than that of ^{99m}Tc-3P-RGD$_2$ (1.45 ± 0.40%ID/g) at 5 min p.i., but this difference disappeared at 60 min p.i. (Figure 4). The tumor uptake of ^{99m}Tc-P6D-RGD$_2$ (2.20 ± 0.42, 2.85 ± 0.55, 3.11 ± 0.47, and 2.45 ± 0.90%ID/g at 5, 30, 60, and 120 min p.i., respectively) was significantly lower ($p < 0.01$) than that of ^{99m}Tc-P6G-RGD$_2$ (9.27 ± 0.72, 8.85 ± 0.67, 8.17 ± 1.10, and 7.82 ± 0.76%ID/g at 5, 30, 60, and 120 min p.i., respectively) over the 2 h study period. In contrast, ^{99m}Tc-P6G-RGD$_2$ and ^{99m}Tc-3P-RGD$_2$ shared similar blood clearance kinetics (Figure 4), and tumor uptake values (7.82−9.27%ID/g for ^{99m}Tc-P6G-RGD$_2$; and 7.24−8.72%ID/g for ^{99m}Tc-3P-RGD$_2$). The kidney uptake of ^{99m}Tc-P6D-RGD$_2$ (Table 1) was also significantly higher ($p < 0.01$) than that of ^{99m}Tc-P6D-RGD$_2$ (Table 2). However, ^{99m}Tc-P6D-RGD$_2$ had the intestine uptake values of 5.86 ± 1.37, 6.58 ± 0.88, 7.08 ± 0.92, and 4.74 ± 0.33%ID/g at 5, 30, 60, and 120 min p.i., respectively, which were much lower ($p < 0.01$) than those of ^{99m}Tc-P6G-RGD$_2$ (11.72 ± 2.01, 9.27 ± 1.15, 6.17 ± 1.55, and 4.74 ± 1.09%ID/g at 5, 30, 60, and 120 min p.i., respectively) over the 2 h study period. Obviously, the linker groups between two cyclic RGD moieties have a significant impact on the blood clearance kinetics (Figure 4), tumor uptake, and biodistribution properties (Figure 5) of ^{99m}Tc-labeled dimeric cyclic RGD peptides.

Integrin $\alpha_v\beta_3$ Specificity. Figure 6A compares the 60 min biodistribution data of ^{99m}Tc-P6D-RGD$_2$ in the athymic nude mice bearing U87MG human glioma xenografts in the absence/presence of excess RGD$_2$. Co-injection of excess RGD$_2$ significantly blocked its tumor uptake (0.30 ± 0.01%ID/g with RGD$_2$ v 3.13 ± 0.47%ID/g without RGD$_2$). There was also a significant blockage of its uptake in several integrin $\alpha_v\beta_3$-positive normal organs by coinjection of excess RGD$_2$. For example, the 60 min uptake values of ^{99m}Tc-P6D-RGD$_2$ in the

Table 1. Selected Biodistribution Data and Tumor-to-Background Ratios of ^{99m}Tc-P6D-RGD$_2$ in Athymic Nude Mice (n = 5) Bearing U87MG Human Glioma Xenografts.[a]

organ	5 min	30 min	60 min	60 min (blocking)	120 min
Blood	4.71 ± 1.00	1.23 ± 0.38	0.49 ± 0.08	0.23 ± 0.01	0.19 ± 0.09
Brain	0.41 ± 0.09	0.25 ± 0.09	0.13 ± 0.02	0.02 ± 0.01	0.11 ± 0.01
Eyes	0.81 ± 0.36	0.89 ± 0.25	0.79 ± 0.31	0.23 ± 0.10	0.54 ± 0.15
Heart	4.23 ± 0.87	2.36 ± 0.24	1.66 ± 0.05	0.20 ± 0.07	1.11 ± 0.16
Intestine	5.86 ± 1.37	6.58 ± 0.88	7.08 ± 0.92	0.22 ± 0.11	4.74 ± 0.33
Kidneys	32.84 ± 7.81	24.67 ± 2.40	19.85 ± 0.28	23.94 ± 3.61	15.43 ± 2.30
Liver	4.26 ± 0.63	3.95 ± 0.11	3.61 ± 0.14	0.28 ± 0.04	2.85 ± 0.51
Lungs	4.46 ± 0.68	2.05 ± 0.28	1.85 ± 0.20	0.29 ± 0.01	1.11 ± 0.42
Muscle	1.63 ± 0.77	1.79 ± 0.20	1.59 ± 0.25	0.18 ± 0.06	0.79 ± 0.23
Spleen	2.70 ± 0.73	2.60 ± 0.37	2.58 ± 0.46	0.14 ± 0.01	2.40 ± 0.37
Tumor	2.20 ± 0.42	2.85 ± 0.55	3.13 ± 0.47	0.30 ± 0.01	2.45 ± 0.90
Tumor/Blood	0.49 ± 0.13	2.50 ± 0.33	6.50 ± 0.58	1.24 ± 0.05	6.98 ± 4.06
Tumor/Liver	0.52 ± 0.10	0.65 ± 0.15	0.87 ± 0.17	1.05 ± 0.09	0.84 ± 0.18
Tumor/Lung	0.49 ± 0.04	1.19 ± 0.35	1.68 ± 0.10	1.10 ± 0.13	2.41 ± 0.73
Tumor/Muscle	1.85 ± 1.08	1.97 ± 0.53	2.00 ± 0.36	1.80 ± 0.11	3.30 ± 1.24

[a]The tumor uptake was expressed as an average plus/minus the standard deviation.

Table 2. Selected Biodistribution Data and Tumor-to-Background Ratios of ^{99m}Tc-P6G-RGD$_2$ in Athymic Nude Mice (n = 5) Bearing U87MG Human Glioma Xenografts[a]

organ	5 min	30 min	60 min	120 min
Blood	0.88 ± 0.05	0.65 ± 0.15	0.56 ± 0.13	0.19 ± 0.02
Brain	0.22 ± 0.03	0.20 ± 0.08	0.15 ± 0.02	0.13 ± 0.02
Eyes	2.24 ± 0.32	2.04 ± 0.15	1.59 ± 0.17	1.22 ± 0.02
Heart	2.39 ± 0.25	1.79 ± 0.11	1.61 ± 0.39	1.02 ± 0.13
Intestine	11.72 ± 2.01	9.27 ± 1.15	6.17 ± 1.55	4.74 ± 1.09
Kidneys	16.62 ± 1.37	12.33 ± 0.86	10.70 ± 1.00	6.64 ± 0.41
Liver	3.09 ± 0.22	2.88 ± 0.25	2.77 ± 0.35	2.22 ± 0.30
Lungs	6.57 ± 0.90	4.38 ± 0.55	3.83 ± 0.56	2.81 ± 0.36
Muscle	1.99 ± 0.72	1.75 ± 0.24	1.68 ± 0.33	0.83 ± 0.11
Spleen	3.37 ± 0.75	3.08 ± 0.88	2.68 ± 0.57	2.31 ± 0.27
Tumor	9.27 ± 0.72	8.85 ± 0.67	8.17 ± 1.10	7.82 ± 0.76
Tumor/Blood	12.17 ± 1.12	14.11 ± 1.25	15.64 ± 2.79	41.76 ± 5.13
Tumor/Liver	3.04 ± 0.27	2.95 ± 0.33	2.86 ± 0.30	3.21 ± 0.53
Tumor/Lung	1.41 ± 0.17	2.07 ± 0.15	2.35 ± 0.24	2.71 ± 0.12
Tumor/Muscle	4.50 ± 1.34	5.04 ± 0.68	5.09 ± 0.51	9.42 ± 1.25

[a]The tumor uptake was expressed as an average plus/minus the standard deviation.

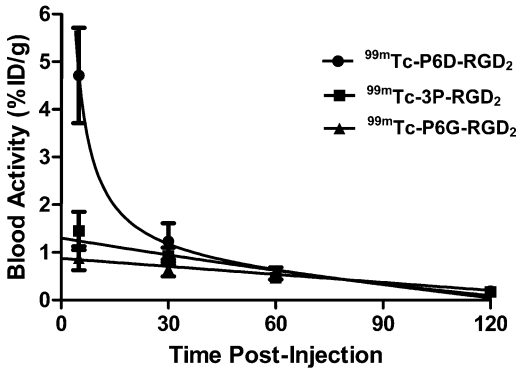

Figure 4. Comparison of the blood radioactivity accumulation of ^{99m}Tc-P6D-RGD$_2$, ^{99m}Tc-P6G-RGD$_2$, and ^{99m}Tc-3P-RGD$_2$ in the athymic nude mice bearing U87MG glioma xenografts to illustrate the impact of linkers (D_3 versus G_3 and PEG_4) between the two c(RGDfK) moieties on blood clearance kinetics of ^{99m}Tc-labeled cyclic RGD peptide dimers.

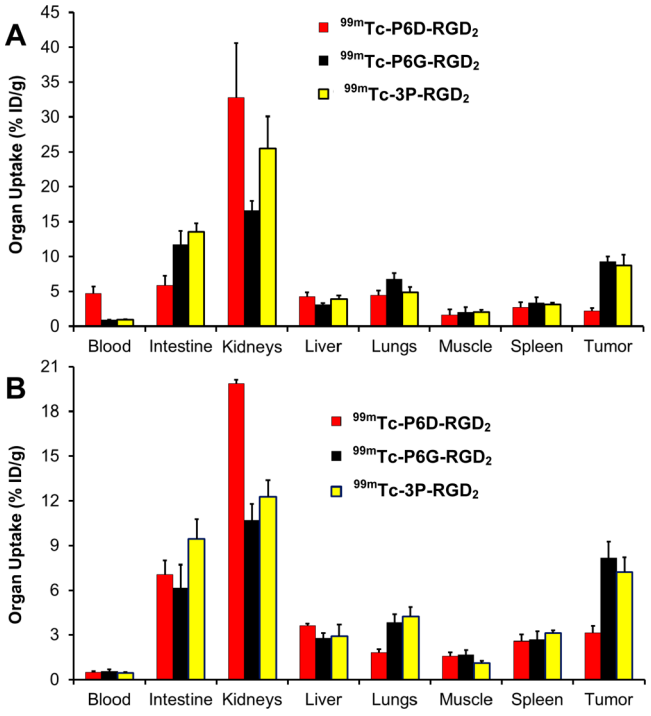

Figure 5. Direct comparison of the selected 5 min (A) and 60 min (B) biodistribution data between ^{99m}Tc-P6D-RGD$_2$, ^{99m}Tc-P6G-RGD$_2$, and ^{99m}Tc-3P-RGD$_2$ in athymic nude mice bearing U87MG glioma xenografts to illustrate the impact of linkers (D_3 versus G_3 and PEG_4) between the two c(RGDfK) moieties on the uptake of ^{99m}Tc-labeled cyclic RGD peptide dimers in tumor and normal organs.

intestine, lungs, and spleen was 7.08 ± 0.92, 1.85 ± 0.20, and 2.58 ± 0.46%ID/g, respectively, without RGD$_2$, while its uptake in the same organs was only 0.22 ± 0.11, 0.29 ± 0.01, and 0.14 ± 0.01%ID/g, respectively, in the presence of excess RGD$_2$. These data clearly showed that the tumor uptake of ^{99m}Tc-P6D-RGD$_2$ is integrin $\alpha_v\beta_3$-specific. A similar conclusion could also be made on the basis of planar imaging data (Figure 6B) of the U87MG glioma-bearing mice in the absence/presence of excess RGD$_2$.

SPECT/CT Imaging and Immunohistochemistry Data. We obtained the SPECT/CT images (Figure 7A) of the athymic nude mice bearing xenografted U87MG glioma and MDA-MB-231 breast tumor administered with ~37 MBq of ^{99m}Tc-P6G-RGD$_2$. We were interested in ^{99m}Tc-P6G-RGD$_2$ because of its higher tumor uptake than that of ^{99m}Tc-P6D-RGD$_2$. It was found that the tumors were clearly visualized with excellent contrast in both animal models. Its tumor uptake was ~8.2%ID/cm^3 in the U87MG glioma and 3.5%ID/cm^3 in the MDA-MB-231 breast tumor on the basis of SPECT quantification. To explain the uptake difference between U87MG and MDA-MB-231 tumors, we obtained microscopic images (Figure 7B) of selected tumor slice stained with anti-integrin β_3 (red color) and anti-CD31 (green color) antibody. CD31 was used as a biomarker for tumor blood vessels (both mature and neovasculature), and was visualized with FITC (green). Integrin β_3 was visualized with Cy3 (red). Yellow color (red β_3 staining verged with green CD31 staining) in overlay images indicates the presence of integrin $\alpha_v\beta_3$ on neovasculature. It was clear that integrin $\alpha_v\beta_3$ was highly expressed on U87MG glioma cells and neovasculature, which was in complete agreement with the high uptake of ^{99m}Tc-P6G-RGD$_2$ in U87MG glioma tumors (Figure 7A). In contrast, the xenografted MDA-MB-231 breast tumors had relatively high

dx.doi.org/10.1021/bc500309r | Bioconjugate Chem. 2014, 25, 1720−1729

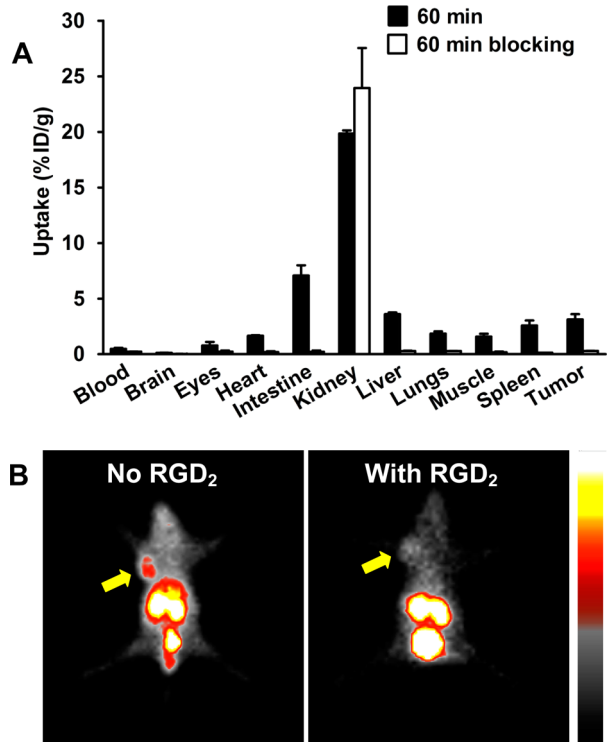

Figure 6. Selected 60 min biodistribution (A) and planar imaging (B) data for ^{99m}Tc-P6D-RGD$_2$ in the athymic nude mice bearing U87MG human glioma xenografts with/without coinjection of RGD$_2$ (350 μg/mouse or 14 mg/kg) to demonstrate its integrin $\alpha_v\beta_3$ specificity. Yellow arrows indicate the presence of U87MG glioma tumors.

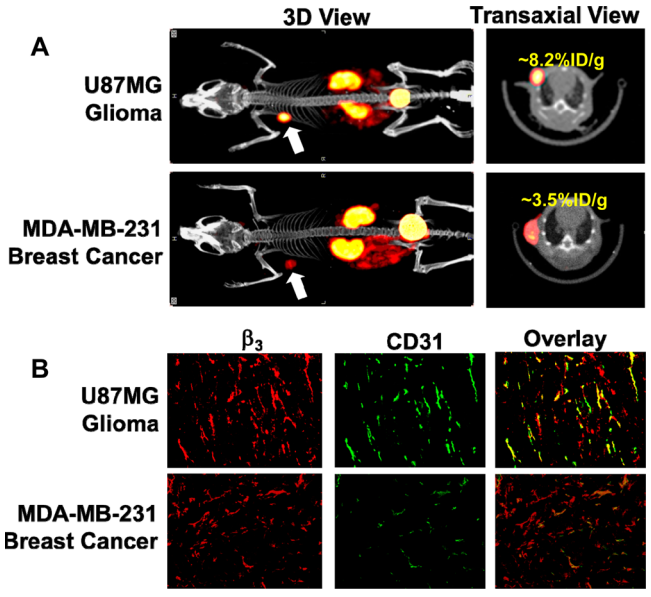

Figure 7. (A) 3D and transverse views of SPECT/CT images of the athymic nude mice bearing U87MG glioma and MDA-MB-231 breast tumor xenografts. Each animal was administered with ~37 MBq of ^{99m}Tc-P6G-RGD$_2$. SPECT/CT study was designed to illustrate their potential utility for tumor imaging. (B) Selected microscopic images (Magnification: 200×) of the tumor slice stained with hamster anti-integrin β_3 (red) and rat anti-CD31 (green) antibodies. Yellow or orange color (red integrin β_3 staining merged with green CD31 staining) indicates the presence of integrin $\alpha_v\beta_3$ on the tumor neovasculature.

expression of integrin $\alpha_v\beta_3$ on tumor cells with limited integrin $\alpha_v\beta_3$ expression on neovasculature, as indicated by the lack of yellow and orange colors in overlay images. As a result, ^{99m}Tc-P6G-RGD$_2$ had lower uptake in the MDA-MB-231 breast tumors than that in U87MG glioma (Figure 7A).

DISCUSSION

There are two biologically important interactions (Chart 1: receptor binding and protein binding) once a radiotracer is injected into the blood circulation. Receptor binding is necessary for the radiotracer to selectively localize in the targeted organ or tissue (e.g., tumor). Higher receptor binding affinity will lead to more radiotracer initial tumor uptake with a longer tumor retention time. Protein bonding is often detrimental because it will reduce the number of radiotracer molecules available for receptor binding, and result in more initial blood radioactivity accumulation (Chart 1). Therefore, the protein bonding should be minimized for the receptor-based target-specific radiotracers. In addition, more hydrophilic radiotracers tend to increase renal excretion, which will lead to lower background radioactivity in the blood pool and normal organs (e.g., liver, lungs, and muscle) with better target-to-background ratios. In contrast, more lipophilic radiotracers tend to have extensive metabolism, which often results in lower tumor uptake with poorer target-to-background ratios.

In this study, we found that the negative charges had very little impact on integrin $\alpha_v\beta_3$ binding affinity of HYNIC-conjugated cyclic RGD dimers (Figure 2: IC_{50} = 40 ± 6 nM for HYNIC-P6D-RGD$_2$; and IC_{50} = 32 ± 5 nM for HYNIC-P6G-RGD$_2$). However, they have a dramatic impact on the blood clearance kinetics (Figure 4), tumor uptake, and biodistribution (Figure 5) of their ^{99m}Tc radiotracers (^{99m}Tc-P6D-RGD$_2$ versus ^{99m}Tc-P6G-RGD$_2$). Therefore, this difference is most likely related to their overall molecular charge and their protein binding capability.

P6D-RGD$_2$ contains two D_3 tripeptide sequences with six carboxylic groups. Due to their low pK_a values (4.5−5.0 for aliphatic acids), they are all expected to be deprotonated under physiological conditions (pH = 7.4). ^{99m}Tc-P6D-RGD$_2$ has a total of nine negative molecular charges (Chart 1), which provide a strong driving force to interact with the positively charged amino residues, such as arginine and lysine. The stronger protein binding leads to higher initial blood activity level (Figure 4), lower tumor uptake and higher kidney uptake of ^{99m}Tc-P6D-RGD$_2$ than those of both ^{99m}Tc-P6G-RGD$_2$ and ^{99m}Tc-3P-RGD$_2$ (Figure 5), in which the G_3 and PEG_4 linkers are neutral under physiological conditions.

One might ask why one D_3 linker is able to minimize the liver uptake of ^{99m}Tc-labeled c(RGDfK),[49] while ^{99m}Tc-P6G-RGD$_2$ has such a high initial blood activity level (Figure 4). The answer lies in the differences of their overall negative molecular charges. In ^{99m}Tc-labeled c(RGDfK), the D_3 linker offers only three negative charges, which was not sufficient for strong protein binding. In ^{99m}Tc-P6D-RGD$_2$, the combination of two D_3 linkers with the triple-charged TPPTS yields a total of nine negative charges. As a result, ^{99m}Tc-P6D-RGD$_2$ is able to form a stronger protein binding (Chart 1), leading to high initial blood radioactivity (Figure 4) and low tumor uptake (Figure 5). It must be noted that protein binding is reversible, and the protein-bound ^{99m}Tc-P6D-RGD$_2$ became dissociated. It is not surprising that all three radiotracers shared almost identical blood radioactivity levels at 60 min p.i. (Figure 4).

dx.doi.org/10.1021/bc500309r | Bioconjugate Chem. 2014, 25, 1720−1729

Chart 1. Schematic Illustration of Biological Interactions and Elimination Routes of ^{99m}Tc-P6D-RGD$_2$

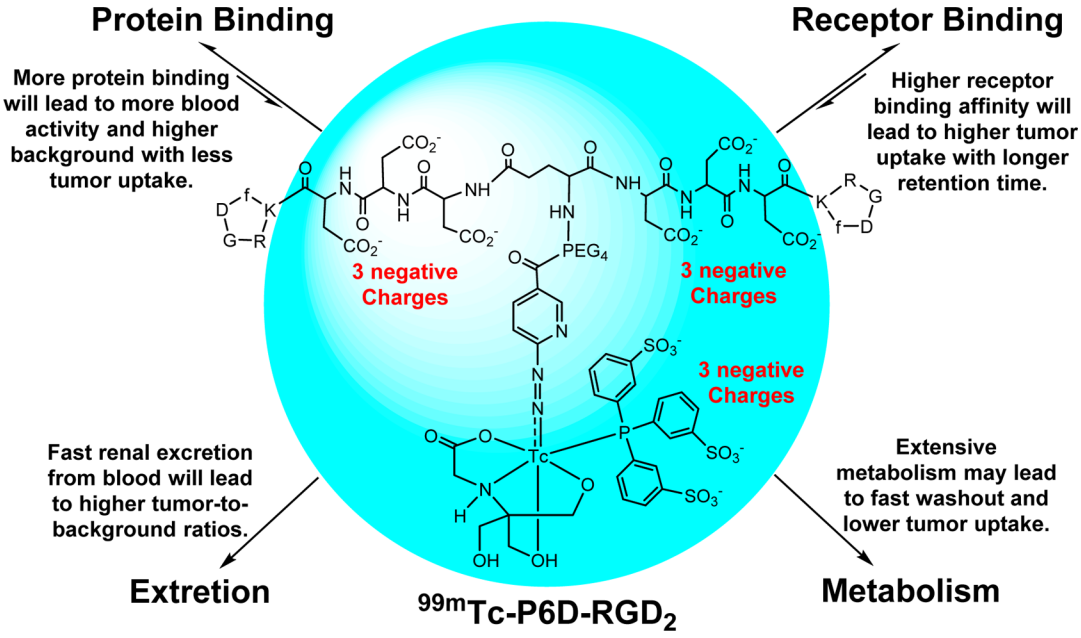

It remains unknown which protein ^{99m}Tc-P6D-RGD$_2$ is bonded to. However, albumin is the most abundant protein in the blood plasma.[53−55] The normal concentration range is 35−50 g/L for human serum albumin (HSA). HSA consists of three homologous domains (I, II, and III) and each domain is formed by two subdomains (A and B).[53,54] The results from X-ray analysis of different ligand−HSA complexes showed the existence of two binding sites in the II and III domains. Subdomains IIA and IIIA contain deep pockets, the entrance of which is surrounded by positively charged amino acid residues.[54] Thus, these pockets are potential binding sites for ^{99m}Tc-P6D-RGD$_2$. If the radiotracer contains multiple negative charges (e.g., two D_3 linkers in ^{99m}Tc-P6D-RGD$_2$), the interaction between radiotracer and albumin may become significant. This might explain why ^{99m}Tc-P6D-RGD$_2$ has much higher initial blood radioactivity than ^{99m}Tc-P6G-RGD$_2$ and ^{99m}Tc-3P-RGD$_2$ (Figure 4) while the D_3 linker is able to reduce the liver uptake for ^{99m}Tc-labeled c(RGDfK).[49]

^{99m}Tc-P6D-RGD$_2$ is not a good radiotracer for tumor imaging due to its high protein binding and low tumor uptake. However, this finding may have important applications in the design of albumin-targeted contrast agents for magnetic resonance imaging (MRI) angiography.[56−58] For the receptor-based radiotracers, protein binding will reduce the number of radiolabeled biomolecules for receptor binding and the radiotracer uptake in the targeted tissues. For albumin-targeted contrast agents, albumin binding will reduce the tumbling rate of Gd(III) chelates, increase the relaxivity of Gd(III) contrast agents, and decrease the doses administered to each subject.[58]

Despite its low uptake in U87MG glioma tumors, the tumor uptake of ^{99m}Tc-P6D-RGD$_2$ was integrin $\alpha_v\beta_3$-specific, as illustrated by the blocking experiments (Figure 6). SPECT/CT data clearly shows the tumor-targeting capability of ^{99m}Tc-P6G-RGD$_2$, and its uptake is dependent on the integrin $\alpha_v\beta_3$ expression levels on tumor cells and neovasculature (Figure 7). If the integrin $\alpha_v\beta_3$ expression level is high on both tumor cells and neovasculature, ^{99m}Tc-P6G-RGD$_2$ will have high tumor uptake. If the integrin $\alpha_v\beta_3$ expression level is low on either tumor cells or tumor neovasculature, the tumor uptake of ^{99m}Tc-P6G-RGD$_2$ will be lower. Therefore, ^{99m}Tc-P6G-RGD$_2$ has the potential as a screening tool for cancer patients before the anti-$\alpha_v\beta_3$ treatment.

CONCLUSION

The most important finding of this study is that the multiple negative charges have a significant detrimental effect on the blood clearance kinetics and tumor uptake of ^{99m}Tc-labeled dimeric cyclic RGD peptides. As a result of its higher protein binding, ^{99m}Tc-P6D-RGD$_2$ had much lower tumor uptake than ^{99m}Tc-P6G-RGD$_2$.

EXPERIMENTAL SECTION

Materials and Instruments. Common chemicals and solvents were purchased from Sigma/Aldrich (St. Louis, MO), and were used without further purification. Cyclic peptides, c(RGDyK), E[c(RGDfK)]$_2$ (RGD$_2$), P6D-RGD$_2$ (PEG$_4$-E[c-(RGDfK(D$_3$))]$_2$), and P6G-RGD$_2$ (PEG$_4$-E[c(RGDfK-(G$_3$))]$_2$), and 3P-RGD$_2$ (PEG$_4$-E[c(RGDfK(PEG$_4$))]$_2$) were purchased from Peptides International, Inc. (Louisville, KY). Sodium succinimidyl 6-(2-(2-sulfonatobenzaldehyde)-hydrazono)nicotinate (HYNIC-NHS), HYNIC-RGD$_2$, HYNIC-3P-RGD$_2$, and [^{99m}Tc(HYNIC-3P-RGD$_2$)(tricine)-(TPPTS)] (^{99m}Tc-3P-RGD$_2$) were prepared according to the literature methods.[38,59] Na^{99m}TcO$_4$ was obtained from Cardinal HealthCare (Chicago, IL). The MALDI (matrix-assisted laser desorption ionization) data were collected on an Applied Biosystems Voyager DE PRO mass spectrometer (Framingham, MA), the Department of Chemistry, Purdue University.

HPLC Methods. The semiprep HPLC method (Method 1) used a LabAlliance HPLC system (Scientific Systems, Inc., State College, PA) equipped with a UV/vis detector (λ = 254 nm) and Zorbax C$_{18}$ column (9.4 mm × 250 mm, 100 Å pore size; Agilent Technologies, Santa Clara, CA). The flow rate was 2.5 mL/min with a mobile phase being isocratic with 90% A (0.1% TFA in acetonitrile) and 10% B (0.1% TFA in water) over the first 5 min, followed by a gradient mobile phase going

dx.doi.org/10.1021/bc500309r | Bioconjugate Chem. 2014, 25, 1720−1729

from 90% A and 10% B at 5 min, and to 60% A and 40% B at 20 min. The radio-HPLC method (Method 2) used the LabAlliance HPLC system equipped with a β-ram IN/US detector (Tampa, FL) and Zorbax C_{18} column (4.6 mm × 250 mm, 300 Å pore size; Agilent Technologies, Santa Clara, CA). The flow rate was 1 mL/min. The mobile phase was isocratic for the first 5 min with 90% A (25 mM NH_4OAc, pH = 6.8) and 10% B (acetonitrile), followed by a gradient mobile phase going from 90% A and 10% B at 5 min to 60% A and 60% B at 20 min.

HYNIC-PEG$_4$-E[c(RGDfK(D$_3$))]$_2$ (HYNIC-P6D-RGD$_2$). HYNIC-OSu (5.4 mg, 12 μmol) and P6D-RGD_2 (4.5 mg, 2 μmol) were dissolved in anhydrous DMF (1.5 mL). Upon addition of excess diisopropylethylamine (DIEA: 50 μmol), the reaction mixture was stirred for ~15 days at room temperature. To the reaction mixture was added 2 mL of water. The pH value was adjusted to 3−4 using TFA. The product was separated from the reaction mixture by HPLC (Method 1). Fractions at ~18 min were collected. Lyophilization of the combined fractions afforded HYNIC-P6D-RGD_2 as a white powder. The yield was 2.5 mg (~48%) with >95% HPLC purity. MALDI-MS: m/z = 2557.2 for $[M + H]^+$ (exact mass = 2557.99 calcd. for $[C_{107}H_{147}N_{29}O_{43}S]$).

HYNIC-PEG$_4$-E[c(RGDfK(G$_3$))]$_2$ (HYNIC-P6G-RGD$_2$). HYNIC-NHS (4.6 mg, 11 μmol) and P6G-RGD_2 (5 mg, 2.6 μmol) were dissolved in 2.0 mL of anhydrous DMF. After addition of excess DIEA (50 μmol), the reaction mixture was stirred at room temperature for 3 days. To the reaction mixture was added 2 mL of water after completion of conjugation. The pH value was adjusted to 3−4 using neat TFA. The product was separated from reaction mixture by HPLC (Method 1). The fraction at 20.5 min was collected. Lyophilization of combined fractions afforded HYNIC-P6G-RGD_2 as a white powder. The yield was 2.0 mg (~34%) with >95% HPLC purity. MALDI-MS: m/z = 2209.5 for $[M + H]^+$ (exact mass = 2209.96 calcd. for $[C_{95}H_{135}N_{29}O_{31}S]$).

^{99m}Tc-Labeling. ^{99m}Tc-P6G-RGD_2 and ^{99m}Tc-P6D-RGD_2 were prepared using a kit formulation according to the literature method.[38,39] To a lyophilized vial containing 25 μg of HYNIC-P6G-RGD_2 or HYNIC-P6D-RGD_2, 7 mg TPPTS, 6.5 mg tricine, 40 mg mannitol, 38.5 mg disodium succinate hexahydrate, and 12.7 mg succinic acid was added 1.0−1.5 mL of $Na^{99m}TcO_4$ solution (370−1110 MBq). The reconstituted vial was heated in a boiling water bath for 10−20 min. After radiolabeling, a sample of resulting solution was analyzed by radio-HPLC (Method 2). The radiochemical purity (RCP) was >95% for both ^{99m}Tc-P6D-RGD_2 and ^{99m}Tc-P6G-RGD_2 before being used for imaging and biodistribution studies. The solution stability was monitored by radio-HPLC for 6 h.

Dose Preparation. For biodistribution, doses were prepared by dissolving ^{99m}Tc radiotracer (no HPLC purification) in saline to a concentration of ~1 MBq/mL. Each animal was injected with ~0.1 mL of the dose solution. For SPECT/CT imaging, doses were prepared by dissolving ^{99m}Tc-P6G-RGD_2 (no HPLC purification) in saline to ~370 MBq/mL. In the blocking experiment, RGD_2 was dissolved in the dose solution to 3.5 mg/mL. The resulting dose solution was filtered with a 0.20 μm Millex-LG filter before being injected into animals. Each animal was injected with ~0.2 mL of the dose solution.

Tumor Cell Culture. The U87MG cell line was obtained from ATCC (American Type Culture Collection, Manassas, VA). U87MG cells were cultured in the Minimum Essential Medium, Eagle with Earle's Balanced Salt Solution (non-essential amino acids sodium pyruvate), and were supplemented with 10% fetal bovine serum (FBS, ATCC) and 1% penicillin and streptomycin solution at 37 °C in a humidified atmosphere of 5% CO_2 in air. Cells were grown as monolayers and were harvested or split when they reached 90% confluence to maintain exponential growth.

Integrin $\alpha_v\beta_3$ Binding Assay. The integrin binding affinity of cyclic RGD peptides was assessed via a displacement assay using ^{125}I-echistatin (PerkinElmer, Branford, CT) as the integrin-specific radioligand. Briefly, the filter multiscreen DV plates (Millipore, Billerica, MA) were seeded with 1 × 10^5 U87MG cells in binding buffer (20 mM Tris, 150 mM NaCl, 2 mM $CaCl_2$, 1 mM $MnCl_2$, 1 mM $MgCl_2$, 0.1% (wt/vol) bovine serum albumin; pH 7.4) and ^{125}I-echistatin (0.75−1.0 kBq) in the presence of increasing concentrations of the cyclic RGD peptide, incubated for 2 h at room temperature. After removing unbound ^{125}I-echistatin, the hydrophilic PVDF filters were washed 3× with the binding buffer, and then collected. Radioactivity was determined using a PerkinElmer Wizard 1480 γ-counter (Shelton, CT). Experiments were carried out twice in triplicate. IC_{50} values were calculated by fitting experimental data with nonlinear regression using GraphPad Prism (GraphPad Software, Inc., San Diego, CA), and were reported as an average plus/minus standard deviation.

Animal Models. Biodistribution and imaging studies were performed in compliance with the NIH animal experimentation guidelines (*Principles of Laboratory Animal Care*, NIH Publication No. 86−23, revised 1985). The protocol was approved by the Purdue University Animal Care and Use Committee (PACUC). Female athymic *nu/nu* mice (4−5 weeks) were purchased from Harlan (Indianapolis, IN), and were inoculated subcutaneously with 5 × 10^6 U87MG cells into the shoulder flank of each animal. Four weeks after inoculation, animals were used for biodistribution and imaging studies.

Biodistribution Protocol. Twenty tumor-bearing mice (20−25 g) were randomly selected, and divided into four groups. Each animal was administered ~0.1 MBq of ^{99m}Tc radiotracer by tail vein injection. Five animals were sacrificed by sodium pentobarbital overdose (~200 mg/kg) at 5, 30, 60, and 120 min postinjection (p.i.). Blood, tumors, and normal organs (brain, eyes, heart, spleen, lungs, liver, kidneys, muscle, and intestine) were harvested, washed with saline, dried with absorbent tissue, weighed, and counted on a PerkinElmer Wizard 1480 γ-counter. The blocking experiment was performed using RGD_2 as the blocking agent. Each animal was administered ~0.1 MBq of ^{99m}Tc-P6D-RGD_2 along with ~350 μg (~14 mg/kg) of RGD_2. Biodistribution data (%ID/g) and tumor-to-background (T/B) ratios were all expressed as the average plus/minus standard deviation standard deviation from five animals. Statistical analysis was performed by one-way analysis of variance (ANOVA) followed by the Newman-Keuls test for multiple comparisons. The level of significance was set at $p < 0.05$.

Planar Imaging Protocol. Three animals bearing U87MG glioma xenografts were used for the whole-body planar imaging with ^{99m}Tc-P6D-RGD_2. Tumor-bearing mice were anesthetized with intraperitoneal injection of Ketamine (40−100 mg/kg) and Xylazine (2−5 mg/kg). Each animal was administered ~37 MBq of ^{99m}Tc-P6D-RGD_2 in 0.1 mL of saline solution. Animals were then placed on a custom-made single head gamma camera (Diagnostic Services Inc., NJ) equipped with a parallel-hole, medium-energy, and high-resolution collimator. Static planar

images were acquired at 30, 60, and 120 min p.i. and stored digitally in a 128 × 128 matrix. The acquisition count limits were set at 300 K. In the blocking experiment, ^{99m}Tc-P6D-RGD$_2$ was coinjected with RGD$_2$ (~14 mg/kg or ~350 μg per 25 g tumor-bearing mouse). Such a large excess of RGD$_2$ was used to make sure that the integrin $\alpha_v\beta_3$ binding sites are completely blocked. After planar imaging, the tumor-bearing animals were euthanized by sodium pentobarbital overdose (100−200 mg/kg).

SPECT/CT Imaging. SPECT/CT images were obtained using a u-SPECT-II/CT scanner (Milabs, Utrecht, The Netherlands) equipped with a 0.6 mm multi-pinhole collimator. The glioma-bearing mouse was injected with ~37 MBq of ^{99m}Tc-P6G-RGD$_2$ in 0.1 mL saline via the tail vein. At 60 min p.i., the animal was placed into a shielded chamber connected to an isoflurane anesthesia unit (Univentor, Zejtun, Malta). Anesthesia was induced using an air flow rate of 350 mL/min and ~3.0% isoflurane. After induction of anesthesia, the animal was immediately placed supine on the scanning bed. The air flow rate was then reduced to ~250 mL/min with ~2.0% isoflurane. Rectangular scans in the regions of interest (ROIs) from SPECT and CT were selected on the basis of orthogonal optical images provided by the integrated webcams. After SPECT (75 projections over 30 min per frame, 2 frames), the animal was transferred into the CT scanner and imaged using "normal" acquisition settings (2° intervals) at 45 kV and 500 μA. After CT acquisition, the animal was allowed to recover in a lead-shielded cage.

Image Reconstruction and Data Processing. SPECT reconstruction was performed using a POSEM (pixelated ordered subsets by expectation maximization) algorithm with 6 iterations and 16 subsets. CT data were reconstructed using a cone-beam filtered back-projection algorithm (NRecon v 1.6.3, Skyscan). After reconstruction, the SPECT and CT data were automatically coregistered according to the movement of the robotic stage, and then resampled to equivalent voxel sizes. Co-registered images were further rendered and visualized using the PMOD software (PMOD Technologies, Zurich, Switzerland). A 3D-Guassian filter (0.8 mm fwhm) was applied to smooth noise, and the LUTs (look up tables) were adjusted for good visual contrast. The reconstructed images were visualized as both orthogonal slices and maximum intensity projections.

Radioactivity Quantification. Radiation sources of a known amount of radioactivity were imaged and reconstructed using the same scanning protocol above. A standard curve was generated to correlate the pixel intensities in reconstructed images with the radioactivity measured by a γ-counter. Tumor delineation was performed on CT and SPECT images according to the literature method.[60−63] The amount of radioactivity in each tumor was calculated according to the above-mentioned standard curve. The tumor uptake of ^{99m}Tc-P6G-RGD$_2$ was expressed as the percentage of injected dose per unit volume (%ID/cm^3).

Tumor Tissue Immunohistochemistry. The U87MG tumors were immediately snap-frozen in the OCT (optical cutting temperature) solution, and were then cut into slices (5 μm). After thorough drying, slices were fixed with ice-cold acetone for 10 min, and dried in the air for 20 min. Sections were blocked with 10% goat serum for 30 min, and then were incubated with the hamster anti-integrin β_3 antibody (1:100, BD Biosciences, San Jose, CA) and rat anti-CD31 antibody (1:100, BD Biosciences) for 1 h at room temperature. After incubating with Cy3-conjugated goat anti-hamster and fluorescein isothiocyanate (FITC)-conjugated goat anti-rat secondary antibodies (1:100, Jackson ImmunoResearch Inc., West Grove, PA) and washing with PBS, the fluorescence was visualized with an Olympus fluorescence microscope (Olympus America Inc., Center Valley, PA). All the pictures were taken under 200× magnification. Brightness and contrast adjustments were made equally to all images.

AUTHOR INFORMATION

Corresponding Author

*Phone: 765-494-0236. Fax 765-496-1377. E-mail: liu100@purdue.edu.

Notes

The authors declare no competing financial interest.

ACKNOWLEDGMENTS

This work was supported, in part, by Purdue University, the Challenge Research Award from Purdue Cancer Center, the Indiana Clinical and Translational Sciences Institute funded in part by grant Number TR000006 (Clinical and Translational Award) from the National Institutes of Health, National Center for advancing Translational Science, and R01 CA115883 (S.L.) from the National Cancer Institute.

ABBREVIATIONS

3P-RGD$_2$, PEG$_4$-E[PEG$_4$-c(RGKfD)]$_2$ = PEG$_4$-Glu[cyclo[Arg-Gly-Asp-D-Phe-Lys(PEG$_4$)]]$_2$ (PEG$_4$ = 15-amino-4,7,10,13-tetraoxapentadecanoic acid); HYNIC-OSu, sodium succinimidyl 6-(2-(2-sulfonatobenzaldehyde)hydrazono)nicotinate; MALDI, matrix-assisted laser desorption ionization; MRI, magnetic resonance imaging; PET, positron emission tomography; P6D-RGD$_2$, PEG$_4$-E[c(RGDfK(D$_3$))]$_2$ = PEG$_4$-Glu[cyclo[Arg-Gly-Asp-D-Phe-Lys(Asp-Asp-Asp)]]$_2$); P6G-RGD$_2$, PEG$_4$-E[c(RGDfK(G$_3$))]$_2$ = PEG$_4$-Glu[cyclo[Arg-Gly-Asp-D-Phe-Lys(Gly-Gly-Gly)]]$_2$); RGD$_2$, E[c(RGDfK)]$_2$ = Glu[cyclo(Arg-Gly-Asp-D-Phe-Lys)]$_2$; SPECT, single photon emission computed tomography; ^{99m}Tc-3P-RGD$_2$, [^{99m}Tc(HYNIC-3P-RGD$_2$)(tricine)(TPPTS)] (HYNIC = 6-hydrazinonicotinyl; and TPPTS = trisodium triphenylphosphine-3,3′,3″-trisulfonate); ^{99m}Tc-P6D-RGD$_2$, [^{99m}Tc(HYNIC-P6D-RGD$_2$)-(tricine)(TPPTS)]; ^{99m}Tc-P6G-RGD$_2$, [^{99m}Tc(HYNIC-P6G-RGD$_2$)(tricine)(TPPTS)]

REFERENCES

(1) Folkman, J. (1995) Angiogenesis in cancer, vascular, rheumatoid and other disease. *Nat. Med. 1*, 27−31.

(2) Bello, L., Francolini, M., Marthyn, P., Zhang, J., Carroll, R. S., Nikas, D. C., Strasser, J. F., Villani, R., Cheresh, D. A., and Black, P. M. (2001) $\alpha_v\beta_3$ and $\alpha_v\beta_5$ integrin expression in glioma periphery. *Neurosurgery 49*, 380−389.

(3) Hwang, R., and Varner, J. (2004) The role of integrins in tumor angiogenesis. *Hematol. Oncol. Clin. North Am. 18*, 991−1006.

(4) Jin, H., and Varner, J. (2004) Integrins: roles in cancer development and as treatment targets. *Br. J. Cancer 90*, 561−565.

(5) Zitzmann, S., Ehemann, V., and Schwab, M. (2002) Arginine-glycine-aspartic acid (RGD)-peptide binds to both tumor and tumor-endothelial cells in vivo. *Cancer Res. 62*, 5139−5143.

(6) Haubner, R., Wester, H. J., Weber, W. A., Mang, C., Ziegler, S. I., Goodman, S. L., Senekowitsch-Schmidtke, R., Kessler, H., and Schwaiger, M. (2001) Noninvasive imaging of $\alpha_v\beta_3$ integrin expression using ^{18}F-labeled RGD-containing glycopeptide and positron emission tomography. *Cancer Res. 61*, 1781−1785.

(7) Thumshirn, G., Hersel, U., Goodman, S. L., and Kessler, H. (2003) Multimeric cyclic RGD peptides as potential tools for tumor

targeting: solid-phase peptide synthesis and chemoselective oxime ligation. *Chem.—Eur. J. 9*, 2717−2725.
(8) Poethko, T., Schottelius, M., Herz, M., Haubner, R., Henriksen, G., Schwaiger, M., Wester, H. j., Thumshirn, G., and Kessler, H. (2004) Chemoselective pre-conjugate radiohalogenation of unprotected mono- and multimeric peptides via oxime formation. *Radiochimica. Acta 92*, 317−327.
(9) Poethko, T., Schottelius, M., Thumshirn, G., Hersel, U., Herz, M., Henriksen, G., Kessler, H., Schwaiger, M., and Wester, H. J. (2004) Two-step methodology for high-yield routine radiohalogenation of peptides: ^{18}F-labeled RGD and octreotide analogs. *J. Nucl. Med. 45*, 892−902.
(10) Haubner, R., Kuhnast, B., Mang, C., Weber, W. A., Kessler, H., Wester, H. J., and Schwaiger, M. (2004) [^{18}F] Galacto-RGD: synthesis, radiolabeling, metabolic stability, and radiation dose estimates. *Bioconjugate Chem. 15*, 61−69.
(11) Chen, X., Park, R., Shahinian, A. H., Tohme, M., Khankaldyyan, V., Bozorgzadeh, M. H., Bading, J. R., Moats, R., Laug, W. E., and Conti, P. S. (2004) ^{18}F-labeled RGD peptide: initial evaluation for imaging brain tumor angiogenesis. *Nucl. Med. Biol. 31*, 179−189.
(12) Chen, X., Park, R., Shahinian, A. H., Bading, J. R., and Conti, P. S. (2004) Pharmacokinetics and tumor retention of ^{125}I-labeled RGD peptide are improved by PEGylation. *Nucl. Med. Biol. 31*, 11−19.
(13) Chen, X., Sievers, E., Hou, Y., Park, R., Tohme, M., Bart, R., Bremner, R., Bading, J. R., and Conti, P. S. (2005) Integrin $\alpha_v\beta_3$−targeted imaging of lung cancer. *Neoplasia 7*, 271−279.
(14) Wu, Y., Zhang, X., Xiong, Z., Cheng, Z., Fisher, D. R., Liu, S., Gambhir, S. S., and Chen, X. (2005) MicroPET imaging of glioma integrin $\alpha_v\beta_3$ expression using ^{64}Cu-labeled tetrameric RGD peptide. *J. Nucl. Med. 46*, 1707−1718.
(15) Li, Z. B., Cai, W., Cao, Q., Chen, K., Wu, Z., He, L., and Chen, X. (2007) ^{64}Cu-labeled tetrameric and octameric RGD peptides for small-animal PET of tumor $\alpha_v\beta_3$ integrin expression. *J. Nucl. Med. 48*, 1162−1171.
(16) Wu, Z., Li, Z. B., Chen, K., Cai, W., He, L., Chin, F. T., Li, F., and Chen, X. (2007) MicroPET of tumor integrin $\alpha_v\beta_3$ expression using ^{18}F-labeled PEGylated tetrameric RGD peptide (^{18}F-FPRGD4). *J. Nucl. Med. 48*, 1536−1544.
(17) Liu, Z., Niu, G., Shi, J., Liu, S., Wang, F., Liu, S., and Chen, X. (2009) ^{68}Ga-labeled cyclic RGD dimers with Gly_3 and PEG_4 linkers: promising agents for tumor integrin $\alpha_v\beta_3$ PET imaging. *Eur. J. Nucl. Med. Mol. Imaging 36*, 947−957.
(18) Li, Y., Guo, J., Tang, S., Lang, L., Chen, X., and Perrin, D. M. (2013) One-step and one-pot-two-step radiosynthesis of cyclo-RGD-^{18}F-aryltrifluoroborate conjugates for functional imaging. *Am. J. Nucl. Med. Mol. Imaging 3*, 44−56.
(19) Liu, Z., Liu, S., Wang, F., Liu, S., and Chen, X. (2009) Noninvasive imaging of tumor integrin expression using ^{18}F-labeled RGD dimer peptide with PEG_4 linkers. *Eur. J. Nucl. Med. Mol. Imaging 36*, 1296−1307.
(20) Dijkgraaf, I., Liu, S., Kruijtzer, J. A., Soede, A. C., Oyen, W. J., Liskamp, R. M., Corstens, F. H., and Boerman, O. C. (2007) Effect of linker variation on the in vitro and in vivo characteristics of an ^{111}In-labeled RGD Peptide. *Nucl. Med. Biol. 34*, 29−35.
(21) Dijkgraaf, I., Kruijtzer, J. A., Liu, S., Soede, A. C., Oyen, W. J., Corstens, F. H., Liskamp, R. M., and Boerman, O. C. (2007) Improved targeting of the $\alpha_v\beta_3$ integrin by multimerization of RGD peptides. *Eur. J. Nucl. Med. Mol. Imaging 34*, 267−273.
(22) Doss, M., Kolb, H. C., Zhang, J. J., Bélanger, M. J., Stubbs, J. B., Stabin, M. G., Hostetler, E. D., Alpaugh, R. K., Von Mehren, M., Walsh, J. C., Haka, M., Mocharla, V. P., and Yu, J. Q. (2012) Biodistribution and radiation dosimetry of the integrin marker ^{18}F-RGD-K_5 determined from whole-body PET/CT in monkeys and humans. *J. Nucl. Med. 53*, 787−795.
(23) Nwe, K., Kim, Y. S., Milenic, D. E., Baidoo, K. E., and Brechbiel, M. W. (2012) ^{111}In- and ^{203}Pb-labeled cyclic arginine-glycine-aspartic acid peptide conjugate as an $\alpha_v\beta_3$ integrin-binding radiotracer. *J. Label Compd. Radiopharm. 55*, 423−426.
(24) Pohle, K., Notni, J., Bussemer, J., Kessler, H., Schwaiger, M., and Beer, A. J. (2012) ^{68}Ga-NODAGA-RGD is a suitable substitute for ^{18}F-Galacto-RGD and can be produced with high specific activity in a cGMP/GRP compliant automated process. *Nucl. Med. Biol. 39*, 777−784.
(25) Tsiapa, I., Loudos, G., Varvarigou, A., Fragogeorgi, E., Psimadas, D., Tsotakos, T., Xanthopoulos, S., Mihailidis, D., Bouziotis, P., Nikiforidis, G. C., and Kagadis, G. C. (2013) Biological evaluation of an ornithine-modified ^{99m}Tc-labeled RGD peptide as an angiogenesis imaging agent. *Nucl. Med. Biol. 40*, 262−272.
(26) Haubner, R., and Wester, H. J. (2004) Radiolabeled tracers for imaging of tumor angiogenesis and evaluation of anti-angiogenic therapies. *Curr. Pharm. Des. 10*, 1439−1455.
(27) Meyer, A., Aurenheimer, J., Modlinger, A., and Kessler, H. (2006) Targeting RGD recognizing integrins: drug development, biomaterial research, tumor imaging and targeting. *Curr. Pharm. Des. 12*, 2723−2747.
(28) Liu, S. (2009) Radiolabeled cyclic RGD peptides as integrin $\alpha_v\beta_3$-targeted radiotracers: maximizing binding affinity via bivalency. *Bioconjugate Chem. 20*, 2199−2213.
(29) Dijkgraaf, I., and Boerman, O. C. (2010) Molecular imaging of angiogenesis with SPECT. *Eur. J. Nucl. Med. Mol. Imaging 37* (Suppl 1), S104−S113.
(30) Tateishi, U., Oka, T., and Inoue, T. (2012) Radiolabeled RGD peptides as integrin $\alpha_v\beta_3$−targeted PET tracers. *Curr. Med. Chem. 19*, 3301−3309.
(31) Liu, S., and Edwards, D. S. (2001) Bifunctional chelators for therapeutic lanthanide radiopharmaceuticals. *Bioconjugate Chem. 12*, 7−34.
(32) Liu, S. (2004) The role of coordination chemistry in development of target-specific radiopharmaceuticals. *Chem. Soc. Rev. 33*, 445−461.
(33) Liu, S. (2008) Bifunctional coupling agents for radiolabeling of biomolecules and target-specific delivery of metallic radionuclides. *Adv. Drug Delivery Rev. 60*, 1347−1370.
(34) Harris, T. D., Kalogeropoulos, S., Nguyen, T., Liu, S., Bartis, J., Ellars, C., Edwards, S., Onthank, D., Yalamanchili, P., Robinson, S., Lazewatsky, J., Barrett, J., and Bozarth, J. (2003) Design, synthesis and evaluation of radiolabeled integrin $\alpha_v\beta_3$ receptor antagonists for tumor imaging and radiotherapy. *Cancer Biother. Radiopharm. 18*, 627−641.
(35) Onthank, D. C., Liu, S., Silva, P. J., Barrett, J. A., Harris, T. D., Robinson, S. P., and Edwards, D. S. (2004) ^{90}Y and ^{111}In complexes of DOTA-conjugated integrin $\alpha_v\beta_3$ receptor antagonist: different but biologically equivalent. *Bioconjugate Chem. 15*, 235−241.
(36) Harris, T. D., Cheesman, E., Harris, A. R., Sachleben, R., Edwards, D. S., Liu, S., Bartis, J., Ellars, C., Onthank, D., Yalamanchili, P., Heminway, S., Silva, P., Robinson, S., Lazewatsky, J., Rajopadhye, M., and Barrett, J. (2007) Radiolabeled divalent peptidomimetic vitronectin receptor antagonists as potential tumor radiotherapeutic and imaging agents. *Bioconjugate Chem. 18*, 1266−1279.
(37) Harris, T. D., Kalogeropoulos, S., Nguyen, T., Dwyer, G., Edwards, D. S., Liu, S., Bartis, J., Ellars, C., Onthank, D., Yalamanchili, P., Heminway, S., Robinson, S., Lazewatsky, J., and Barrett, J. (2006) Structure-activity relationships of ^{111}In- and ^{99m}Tc-labeled quinolin-4-one peptidomimetics as ligands for the vitronectin receptor: potential tumor imaging agents. *Bioconjugate Chem. 17*, 1294−1313.
(38) Shi, J., Wang, L., Kim, Y. S., Zhai, S., Liu, Z., Chen, X., and Liu, S. (2008) Improving tumor uptake and excretion kinetics of ^{99m}Tc-labeled cyclic arginine-glycine-aspartic (RGD) dimers with triglycine linkers. *J. Med. Chem. 51*, 7980−7990.
(39) Wang, L., Shi, J., Kim, Y. S., Zhai, S., Jia, B., Zhao, H., Liu, Z., Wang, F., Chen, X., and Liu, S. (2009) Improving tumor-targeting capability and pharmacokinetics of ^{99m}Tc-labeled cyclic RGD dimers with PEG_4 linkers. *Mol. Pharmaceutics 6*, 231−245.
(40) Shi, J., Wang, L., Kim, Y. S., Zhai, S., Jia, B., Wang, F., and Liu, S. (2009) ^{99m}TcO (MAG_2-$3G_3$-dimer): a new integrin $\alpha_v\beta_3$-targeted SPECT radiotracer with high tumor uptake and favorable pharmacokinetics. *Eur. J. Nucl. Med. Mol. Imaging 36*, 1874−1884.

(41) Shi, J., Kim, Y. S., Zhai, S., Liu, Z., Chen, X., and Liu, S. (2009) Improving tumor uptake and pharmacokinetics of ^{64}Cu-labeled cyclic RGD peptide dimers with Gly_3 and PEG_4 linkers. *Bioconjugate Chem. 20*, 750−759.
(42) Chakraborty, S., Shi, J., Kim, Y. S., Zhou, Y., Jia, B., Wang, F., and Liu, S. (2011) Evaluation of ^{111}In-labeled cyclic RGD peptides: tetrameric not tetravalent. *Bioconjugate Chem. 21*, 969−978.
(43) Shi, J., Kim, Y. S., Chakraborty, S., Jia, B., Wang, F., and Liu, S. (2009) 2-Mercaptoacetylglycylglycyl (MAG_2) as a bifunctional chelator for ^{99m}Tc-labeling of cyclic RGD dimers: effect of technetium chelate on tumor uptake and pharmacokinetics. *Bioconjugate Chem. 20*, 1559−1568.
(44) Shi, J., Zhou, Y., Chakraborty, S., Kim, Y. S., Jia, B., Wang, F., and Liu, S. (2011) Evaluation of ^{111}In-labeled cyclic RGD peptides: effects of peptide and linker multiplicity on their tumor uptake, excretion kinetics and metabolic stability. *Theranostics 1*, 322−340.
(45) Shi, J., Kim, Y. S., Chakraborty, S., Zhou, Y., Wang, F., and Liu, S. (2011) Impact of bifunctional chelators on biological properties of ^{111}In-labeled cyclic peptide RGD dimers. *Amino Acids 41*, 1059−1070.
(46) Zhou, Y., Kim, Y. S., Chakraborty, S., Shi, J., Gao, H., and Liu, S. (2011) ^{99m}Tc-labeled cyclic RGD peptides for noninvasive monitoring of tumor integrin $\alpha_v\beta_3$ expression. *Mol. Imaging 10*, 386−397.
(47) Zhou, Y., Kim, Y. S., Lu, X., and Liu, S. (2012) Evaluation of ^{99m}Tc-labeled cyclic RGD dimers: impact of cyclic RGD peptides and ^{99m}Tc chelates on biological properties. *Bioconjugate Chem. 23*, 586−595.
(48) Ji, S., Czerwinski, A., Zhou, Y., Shao, G., Valenzuela, F., Sowiński, P., Chauhan, S., Pennington, M., and Liu, S. (2013) ^{99m}Tc-Galacto-RGD_2: a novel ^{99m}Tc-labeled cyclic RGD peptide dimer useful for tumor imaging. *Mol. Pharmacol. 10*, 3304−3314.
(49) Haubner, R., Bruchertseifer, F., Bock, M., Kessler, H., Schwaiger, M., and Wester, H. J. (2004) Synthesis and biological evaluation of a ^{99m}Tc-labeled cyclic RGD peptide for imaging the $\alpha_v\beta_3$ expression. *Nuklearmedizin 43*, 26−32.
(50) Ma, Q., Ji, B., Jia, B., Gao, S., Ji, T., Wang, X., Han, Z., and Zhao, G. (2011) Differential diagnosis of solitary pulmonary nodules using ^{99m}Tc-3P_4-RGD_2 scintigraphy. *Eur. J. Nucl. Med. Mol. Imaging 38*, 2145−2152.
(51) Zhu, Z., Miao, W., Li, Q., Dai, H., Ma, Q., Wang, F., Yang, A., Jia, B., Jing, X., Liu, S., Shi, J., Liu, Z., Zhao, Z., Wang, F., and Li, F. (2012) ^{99m}Tc-3PRGD_2 for integrin receptor imaging of lung cancer: a multicenter study. *J. Nucl. Med. 53*, 716−722.
(52) Zhao, D., Jin, X., Li, F., Liang, J., and Lin, Y. (2012) Integrin $\alpha_v\beta_3$ imaging of radioactive iodine−refractory thyroid cancer using ^{99m}Tc-3PRGD_2. *J. Nucl. Med. 53*, 1872−1877.
(53) Carter, D. C., and Ho, J. X. (1994) Structure of serum albumin. *Adv. Protein Chem. 45*, 153−203.
(54) Sugio, S., Kashima, A., Mochizuki, S., Noda, M., and Kobayashi, K. (1999) Crystal structure of human serum albumin at 2.5 Å resolution. *Protein Eng. 12*, 439−446.
(55) He, X. M., and Carter, D. C. (1992) Atomic structure and chemistry of human serum albumin. *Nature 358*, 209−215.
(56) Moriggi, L., Yaseen, M. A., Helm, L., and Caravan, P. (2012) Serum albumin targeted, pH-dependent magnetic resonance relaxation agents. *Chem.—Eur. J. 18*, 3675−3686.
(57) Boros, E., and Caravan, P. (2013) Structure-relaxivity relationships of serum albumin targeted MRI probes based on a single amino acid Gd complex. *J. Med. Chem. 56*, 1782−1786.
(58) Pierre, V. C., Allen, M. J., and Caravan, P. (2014) Contrast agents for MRI: 30+ years and where are we going? *J. Biol. Inorg. Chem. 19*, 127−131.
(59) Harris, T. D., Sworin, M., Williams, N., Rajopadhye, M., Damphousse, P. R., Glowacka, D., Poirier, M. J., and Yu, K. (1999) Synthesis of stable hydrazones of a hydrazinonicotinyl-modified peptide for the preparation of ^{99m}Tc-labeled radiopharmaceuticals. *Bioconjugate Chem. 10*, 808−814.
(60) Shao, G., Zhou, Y., Wang, F., and Liu, S. (2013) Monitoring glioma growth and tumor necrosis with the U-SPECT-II/CT scanner by targeting integrin $\alpha_v\beta_3$. *Mol. Imaging 12*, 39−48.
(61) Zhou, Y., Shao, G., and Liu, S. (2012) Monitoring breast tumor lung metastasis by U-SPECT-II/CT with an integrin $\alpha_v\beta_3$-targeted radiotracer ^{99m}Tc-3P-RGD_2. *Theranostics 2*, 577−588.
(62) Ji, S., Zheng, Y., Shao, G., Zhou, Y., and Liu, S. (2013) Integrin $\alpha_v\beta_3$−targeted radiotracer ^{99m}Tc-3P-RGD_2 useful for noninvasive monitoring of breast tumor response to antiangiogenic linifanib therapy but not anti-integrin $\alpha_v\beta_3$ RGD_2 therapy. *Theranostics 3*, 816−830.
(63) Ji, S., Zhou, Y., Voorbach, M. J., Shao, G., Zhang, Y., Fox, J. B., Albert, D. H., Luo, Y., Liu, S., and Mudd, S. R. (2013) Monitoring tumor response to linifanib therapy with SPECT/CT using the integrin $\alpha_v\beta_3$-targeted radiotracer ^{99m}Tc-3P-RGD_2. *J. Pharmacol. Exp. Ther. 346*, 251−258.